Dichroic rugate filters based on birefringent porous silicon

Nobuyuki Ishikura,[1] **Minoru Fujii,**[1,*] **Kohei Nishida,**[1] **Shinji Hayashi,**[1] **and Joachim Diener**[2]

[1]*Department of Electrical and Electronic Engineering, Graduate School of Engineering, Kobe University, Rokkodai, Nada, Kobe 657-8501, Japan*

[2]*Physik-Department E16, Technische Universität München, D-85747 Garching, Germany*
Corresponding author: fujii@eedept.kobe-u.ac.jp

Abstract: Rugate filters made of anisotropically nanostructured birefringent silicon have been fabricated and studied by polarization-resolved transmission measurements. Electrochemical etching of a (110) oriented Si wafer results in porous silicon layers which exhibit a strong in-plane birefringence. We demonstrate that a sinusoidal refractive index variation of birefringent porous silicon combined with index-matching layers and apodization results in a dichroic rugate filter having a stop-band dependent on the polarization direction of the incident light without higher-order harmonics and sidelobes. We also demonstrate that the combination of different dichroic rugate filters allow us to realize filters with more complex properties in a single preparation step.

References and links

1. F. Genereux, S. W. Leonard, H. M. van Driel, A. Birner, and U. Gösele, "Large birefringence in two-dimensional silicon photonic crystals," Phys. Rev. B **63**, 161101 (2001).
2. F. Xu, R. C. Tyan, P. C. Sun, Y. Fainman, C. C. Cheng, and A. Scherer, "Fabrication, modeling, and characterization of form-birefringent nanostructures," Opt. Lett. **20**, 2457–2459 (1995).
3. N. Künzner, D. Kovalev, J. Diener, E. Gross, V. Yu. Timoshenko, G. Polisski, F. Koch, and M. Fujii, "Giant birefringence in anisotropically nanostructured silicon," Opt. Lett. **26**, 1265–1267 (2001).
4. J. Diener, N. Künzner, D. Kovalev, E. Gross, V. Yu. Timoshenko, G. Polisski, and F. Koch, "Dichroic Bragg reflectors based on birefringent porous silicon," Appl. Phys. Lett. **78**, 3887–3889 (2001).
5. J. Diener, N. Künzner, D. Kovalev, E. Gross, F. Koch, and M. Fujii, "Dichroic behavior of multilayer structures based on anisotropically nanostructured silicon," J. Appl. Phys. **91**, 6704–6709 (2002).
6. J. Diener, N. Künzner, E. Gross, D. Kovalev, and M. Fujii, "Planar silicon-based light polarizers," Opt. Lett. **29**, 195–197 (2004).
7. B. G. Bovard, "Rugate filter theory: an overview," Appl. Opt. **32**, 5427–5442 (1993).
8. M. G. Berger, R. Arens-Fischer, M. Thönissen, M. Krüger, S. Billat, H. Lüth, S. Hilbrich, W. Theiß, and P. Grosse, "Dielectric filters made of PS: advanced performance by oxidation and new layer structures," Thin Solid Films **297**, 237–240 (1997).
9. E. Lorenzo, C. J. Oton, N. E. Capuj, M. Ghulinyan, D. Navarro-Urrios, Z. Gaburro, and L. Pavesi, "Porous silicon-based rugate filters," Appl. Opt. **44**, 5415–5421 (2005).
10. M. S. Salem, M. J. Sailor, T. Sakka, and Y. H. Ogata, "Electrochemical preparation of a rugate filter in silicon and its deviation from the ideal structure," J. Appl. Phys. **101**, 063503 (2007).
11. N. Künzner, J. Diener, E. Gross, D. Kovalev, V. Yu. Timoshenko, and M. Fujii, "Form birefringence of anisotropically nanostructured silicon," Phys. Rev. B **71**, 195304 (2005).
12. W. H. Southwell, "Using apodization functions to reduce sidelobes in rugate filters," Appl. Opt. **28**, 5091–5094 (1989).

13. H. A. Abu-Safia, A. I. Al-Sharif, and I. O. Abu Alijarayesh, "Rugate filter sidelobe suppression using half-apodization," Appl. Opt. **32**, 4831–4835 (1993).
14. W. H. Southwell, "Gradient-index antireflection coatings," Opt. Lett. **8**, 584–586 (1983).
15. M. Born and E. Wolf, *Principles of Optics* (Cambridge University Press, 1999).
16. J. A. Dobrowolski and D. Lowe, "Optical thin film synthesis program based on the use of Fourier transforms," Appl. Opt. **17**, 3039–3050 (1978).
17. A. G. Imenes and D. R. McKenzie, "Flat-topped broadband rugate filters," Appl. Opt. **45**, 7841–7850 (2006).
18. W. H. Southwell, "Extended-bandwidth reflector designs by using wavelets," Appl. Opt. **36**, 314–318 (1997).

1. Introduction

The combination of electronic and photonic elements in an integrated circuit requires Si processing technology that allows optical elements to be integrated on a Si wafer. Polarizing elements are one of the most important optical elements in the optoelectronic circuits. One problem with realizing polarizing elements from crystalline Si is that its intrinsic birefringence and hence its ability to influence polarized light is small. Therefore, birefringence of Si-based materials has been achieved by the anisotropic nanostructuring. For example, periodic nanostructures like two-dimensional photonic crystals [1] and gratings [2] exhibit large birefringence. Another approach leading to birefringence of Si is electrochemical etching of a low symmetry, e.g. (110), surface of a Si wafer. Electrochemical etching of a (110) Si wafer results in the formation of Si nanowire skeletons (porous silicon: PSi) aligned in a certain direction. The alignment of Si nanowire skeletons exhibit a strong in-plane birefringence in a very wide wavelength range covering the visible to near infrared region [3]. Because of the reduced size of Si nanowires and voids smaller than several tenth of nm, birefringent PSi is considered to be a quasicontinuous optical medium. The important advantage of birefringent PSi to realize various optical components is its simplicity to modulate the refractive index. The refractive index and the thickness can be controlled precisely by the etching current density and time. Therefore, a stack of birefringent PSi layers with alternating refractive indices and thicknesses can easily be produced and they result in a dichroic Bragg reflector with a stop-band depending on the polarization direction of the incident light [4, 5].

Although some planar polarizing elements can be realized by the stack of the birefringent PSi layers [6], the performance is limited by the appearance of unnecessary higher-order harmonics and interference oscillations (sidelobes). The problem can be solved by employing a so-called rugate filter. A rugate filter is a kind of interference filter characterized by a continuous sinusoidal refractive index variation in the direction perpendicular to the film plane [7]. Compared with Bragg reflectors, rugate filters provide advantages of suppressed higher-order harmonics and sidelobes. The general drawback of the rugate filter is its difficulty in realizing the complex refractive index profile with a great accuracy. PSi is an almost ideal material to realize a rugate filter because a smooth refractive index profile can easily be achieved by simply modulating the current density continuously. In fact, PSi-based rugate filters have been demonstrated by some groups [8, 9, 10]. However, the previous work was limited for PSi made from (100) Si wafers, which does not show in-plane birefringence. The purpose of this work is to realize dichroic rugate filters by using birefringent PSi. We demonstrate that a sinusoidal refractive index variation of birefringent PSi combined with index-matching layers and apodization results in dichroic rugate filters without higher-order harmonics and sidelobes.

2. Experimental details

PSi structures were produced by electrochemical etching of (110) oriented p$^+$ Si wafers (1-5 mΩ·cm). The etching was performed at room temperature in a solution of 1:1 by volume mixture of HF (46wt.% in water) and ethanol. To vary the porosity of the layers (and therefore their mean refractive indices) the current density was changed from 20 mA/cm^2 to 100 mA/cm^2

by computer-controlled current source (Agilent 6612C). The rugate refractive index profiles were realized by stepwise current variation with the minimum step of 0.5 mA/cm^2. During the etching process, several etch-stop steps of zero current were inserted to recover the HF concentration at the dissolution front. At the end of the etching process a high current pulse (400 mA/cm^2, 1.6 s) was applied to detach PSi structures from the substrate. Transmittance spectra of the prepared samples were measured by a UV-visible-NIR spectrophotometer (Shimadzu UV-3101PC) over the spectral range of 350 to 2300 nm with the spectral resolution of 1 nm. The incident light was linearly polarized with a Glan-Thompson prism and directed normally onto the sample with polarization vector (**E**) aligned either parallel to the [001] or to the [1 $\bar{1}$0] crystallographic directions in the (110) surface plane.

3. Results and discussion

3.1. Optical constants of a single optically anisotropic PSi layer

For design and fabrication of a PSi based rugate filter, the correlation between the optical constants and electrochemical etching condition is necessary. To obtain etching rates and refractive indices as a function of the etching current density, (110) PSi monolayers were prepared at constant current densities ranging from 20 mA/cm^2 to 100 mA/cm^2. The etching rates (Fig. 1(a)) are obtained from the layer thickness estimated by cross-sectional scanning electron microscopy (SEM).
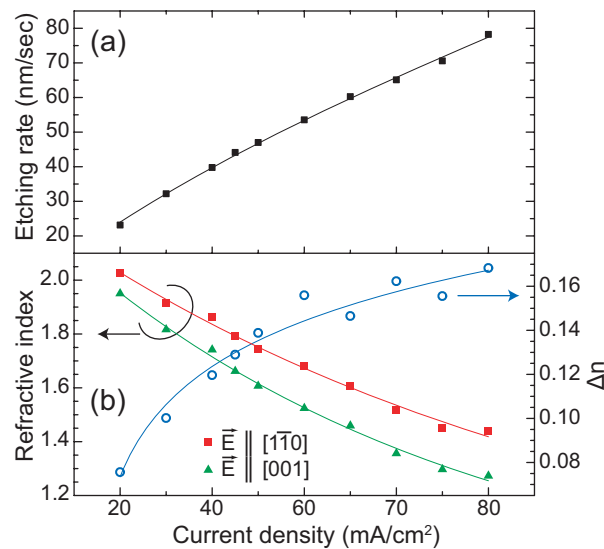

Fig. 1. (a) Etching rate of a (110) oriented p$^+$ Si wafer as a function of current density. (b) Refractive indices and optical anisotropy (Δn) for single layers of (110) PSi estimated from the interference fringes for **E** $\parallel$ [001] and **E** $\parallel$ [1$\bar{1}$0] as a function of current density.

To determine the refractive index, the polarization-resolved transmittance spectra of the single layers were recorded. From the spectral position of the interference fringes for **E** $\parallel$ [001] and **E** $\parallel$ [1$\bar{1}$0] the corresponding refractive indices ($n_{[001]}$ and $n_{[1\bar{1}0]}$) are deduced according to the simple relation;

$$n = \frac{1}{2d} \left(\frac{1}{\lambda_r} - \frac{1}{\lambda_{r+1}} \right)^{-1} \tag{1}$$

where d denotes the thickness of the PSi layer, n is the refractive index, and λ_r is the wavelength

of the rth fringe. The calculated refractive indices (at wavelength of 2μm) and the anisotropy ($\Delta n = n_{[1\bar{1}0]} - n_{[001]}$) are shown in Fig. 1(b). The in-plane optical anisotropy of the layers is evident: the refractive index for **E** parallel to the $[1\bar{1}0]$ direction is substantially larger than that to the $[001]$ direction. As seen in Fig. 1(b), the value of the optical anisotropy (Δn) rises as the current density increases and the maximum value reaches $\simeq 0.17$ comparable to that of natural birefringent crystals such as calcite.

3.2. Cross-sectional TEM observation of a dichroic rugate filter

Figure 2 shows cross-sectional TEM images of a typical rugate filter made from a (110) Si wafers observed from a $[1\bar{1}2]$ direction (Fig. 2(a)). The refractive index profile is the same as that shown in Fig. 3(a). The details will be explained later. A smooth periodic structure can be seen in Fig. 2(b). The black and white contrast is due to the repetition of low and high porosity layers, respectively. In Fig. 2(c), we can see that the transition from the dark and the bright region is gradual (not abrupt) due to the rugate structure. Figure 2(d) shows a higher resolution image. The dark regions correspond to PSi skeletons (Si nanowires), while the bright regions to pores. We can clearly see that the nanowires are not aligned to the direction of etching due to preferential etching of Si to the $<100>$ directions. The alignment of nanowires into specific directions causes the birefringence. Details of the mechanism of the birefringence can be found in our previous paper [11]. In Fig. 2(d) the width of nanowires is about 10 nm and that of pores is about 20 nm. These are more than two orders of magnitude smaller than the wavelength of near infrared light, and thus scattering loss is considered to be negligibly small.

3.3. Dichroic rugate filters

The rugate refractive index profile used in this work is expressed as

$$n(x) = \exp\left[\frac{\ln n_H + \ln n_L}{2} + \frac{\ln n_H - \ln n_L}{2}\sin\left(\frac{4\pi x}{\lambda_0} + \phi\right)\right] \qquad (2)$$

where x is the optical path length, n_H and n_L are maximum and minimum refractive indices used in the layer, λ_0 is the wavelength of the stop-band position, and ϕ is the phase angle [7, 9].
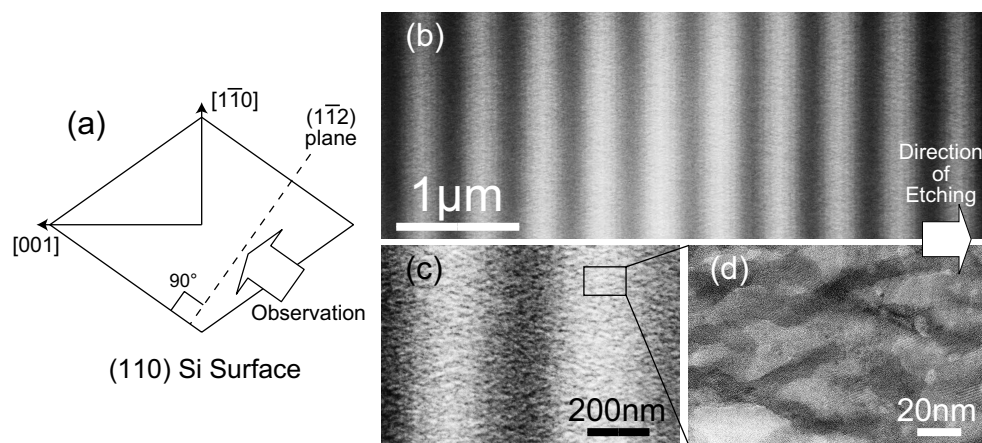

Fig. 2. Cross-sectional TEM images of a rugate filter made from a (110) Si wafer observed from a $[1\bar{1}2]$ direction (a). The magnification factors are (b)10^4, (c)5×10^4 and (d)4×10^5, respectively.

Such a sinusoidal profile would result in the reflection band without higher-order harmonics. However, as a result of the sharp truncation of the refractive index profile at the boundaries of the filter, a simple sinusoidal index profile would also generate interference oscillation (sidelobes) appearing on both sides of the stop-band. To reduce these unnecessary sidelobes, we introduce apodization that is a well-known technique for eliminating sidelobes coming from truncation [12]. We chose a $\sin(x)$ apodization function from 0 to π, which shows good sidelobes suppression properties with high stop-band rejection level. A half-apodization technique [13] is also used to reduce total etching time [9]. Furthermore, to remove sidelobes caused by large refractive index mismatch between the rugate structure and the surrounding media, the quintic index-matching layers are added to the front and back of the filter. The refractive index profile of the quintic index-matching layer [14] that matches indices form n_1 to n_2 is expressed as

$$n(t) = n_1 + (n_2 - n_1)(10t^3 - 15t^4 + 6t^5) \tag{3}$$

where t is the normalized layer thickness, which varies from 0 to 1.

The etching rate and the refractive index shown in Fig. 1 are used to realize a rugate refractive index profile. In birefringent PSi, however, the refractive index in the [001] and [1 $\bar{1}$0] directions cannot be controlled independently and thus optimization of the structure in both directions is
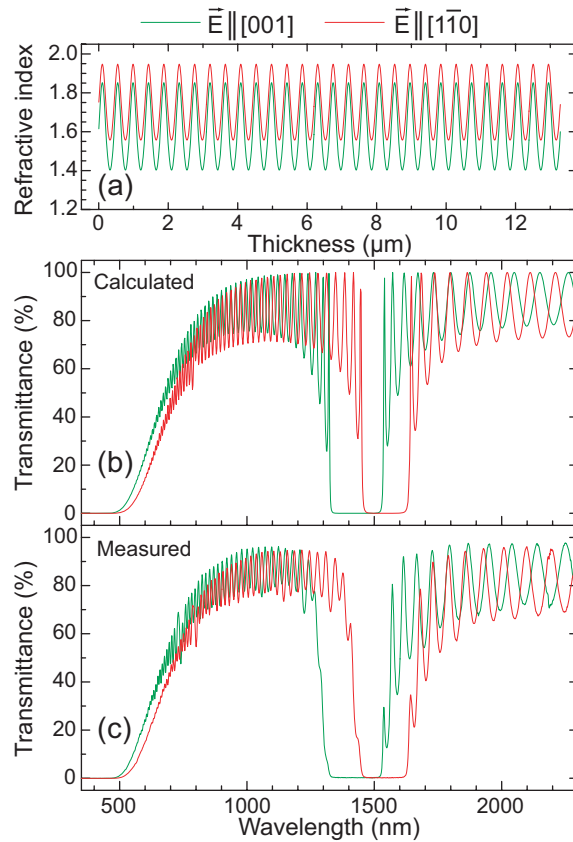

Fig. 3. A dichroic rugate filter with 30 periods: (a) refractive index profiles versus physical depth, (b) calculated and (c) measured polarization-resolved transmittance spectra for **E** ∥ [001] and **E** ∥ [1$\bar{1}$0]. The maximum optical density at the center of the stop-band is 2.7 for both polarization directions.

very difficult. Furthermore, strong etching current density dependence of Δn makes the structure design more difficult. In this work, as a compromise, we employ an average refractive index $n_{mid} = (n_{[1\bar{1}0]} + n_{[001]})/2$ to design the structure.

Figure 3(a) shows the refractive index profiles of a 30 periods (110) rugate filter for $\mathbf{E}$ parallel to the $[1\bar{1}0]$ and $[001]$ crystallographic directions. Figures 3(b) and (c) show the calculated and measured polarization-resolved transmittance spectra of the (110) rugate filter, respectively. The calculation is made by a transfer matrix method [15] by taking into account the wavelength dispersion of the refractive index. Contrary to standard PSi-based rugate filters [8, 9, 10] the spectral position of a stop-band depends on the polarization direction of the incident light. For $\mathbf{E} \parallel [001]$ the stop-band appears around 1430 nm but is significantly shifted towards longer wavelength ($\sim$1540 nm) for $\mathbf{E} \parallel [1\bar{1}0]$. On the both sides of the stop-band, one can see strong sidelobes in both the measured and the calculated spectra. The sidelobes for $\mathbf{E} \parallel [1\bar{1}0]$ are slightly larger because the refractive index mismatch between the rugate structure and the surrounding media is larger than that for $\mathbf{E} \parallel [001]$. A very weak second-harmonic peak and good coincidence between the experimental and calculated transmittance spectra indicate that the
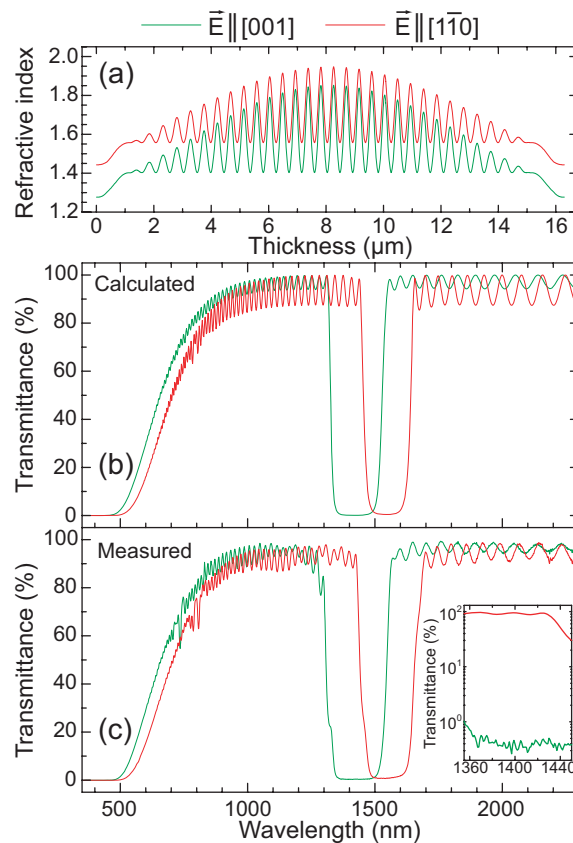

Fig. 4. An apodized dichroic rugate filter with 30 periods and index-matching layers: (a) refractive index profiles versus physical depth, (b) calculated and (c) measured polarization-resolved transmittance spectra for $\mathbf{E} \parallel [001]$ and $\mathbf{E} \parallel [1\bar{1}0]$. The optical density is 2.5 for $\mathbf{E} \parallel [001]$ and 2.2 for $\mathbf{E} \parallel [1\bar{1}0]$ at the center of the stop-band. Inset shows polarization-resolved transmittance spectra of the same structure in the spectral range from 1355 to 1450 nm.

etching process is well controlled.

Figure 4(a) shows a refractive index profiles of an apodized (110) rugate filter with index-matching layers. The calculated and measured transmittance spectra are shown in Figs. 4(b) and (c), respectively. We can see strong suppression of the sidelobes because of the apodization and the presence of index-matching layers. The width of the stop-band decreases by about 30% compared with that of the nonapodized sample, because apodization usually reduces the bandwidth. Inset of Fig. 4(c) shows the polarization-resolved transmission spectra in the spectral range from 1355 to 1450 nm. For this specific spectral range light polarized along the [001] direction is reflected while that light polarized along the [1 $\bar{1}$0] direction passes the whole structure. Since the [001] and [1 $\bar{1}$0] directions are orthogonal in the (110) Si surface plane, the transmitted light is linearly polarized, i.e. this rugate filter acts as a planar linear polarizer. Due to the small sidelobes and high reflectance, the extinction ratio is better than 20 dB (up to 25 dB) over the wavelength range and the transmittance is very high.

3.4. Narrow bandwidth dichroic rugate filter

For high quality dichroic structures it is essential that both stop-bands do not overlap. The separation of the rugate filter stop-bands can be achieved by reducing its bandwidth. The width of the stop-band is determined by the index contrast of the rugate filter. Therefore, we fabricate a rugate filter with smaller contrast to demonstrate the separated stop-bands. Figure 5(a) shows the refractive index profiles of the reduced contrast rugate filter. Compared to the dichroic rugate filter shown in Fig. 4(a) the refractive index contrasts of this narrow bandwidth rugate filter are reduced from 1.4-1.85 (1.56-1.95) to 1.4-1.63 (1.56-1.77) for $\mathbf{E} \parallel$ [001] ([1 $\bar{1}$0]). To compensate small reflectance arising from the low refractive index contrast, the periods are increased to 70. The measured polarization-resolved transmittance spectra are shown in Fig. 5(b). The bandwidth for both polarization directions of incident light are successfully reduced and the stop-bands are fully spectrally separated, while sidelobes and harmonics are kept very
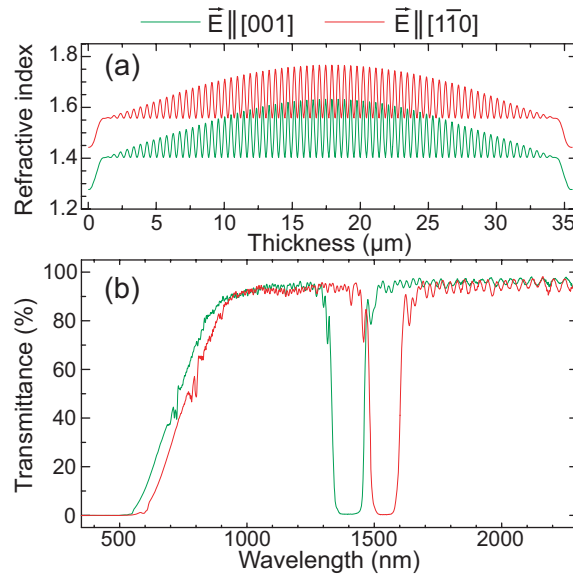

Fig. 5. Narrow bandwidth dichroic rugate filter with 70 periods: (a) refractive index profiles versus physical depth, (b) calculated and (c) measured polarization-resolved transmittance spectra for $\mathbf{E}$ parallel to the [1 $\bar{1}$0] and [001] directions.

low. Since the separation of the stop-bands is determined by the birefringence level (Δn) of the structure [5], the spectral splitting can be adjusted by changing the average refractive index of the structure utilizing the large variation of Δn shown in Fig. 1(b).

3.5. *Double band dichroic rugate filter*

Because of the flexibility of the graded index approach, it is possible to reflect multiple wavelengths by combining two rugate filter designs. The multiple-line rugate filters can be usually realized in three different methods. The first method is based on the superposition principle for waves, whereby rugate profiles of different periodicity may be added together to form one complex waveform [16]. The second method is based upon the serial method [17], in which stacks of different periodicity are deposited one after the other. The third method is the combination principle of the superposition and the serial methods, resulting in the reduction of the total film thickness [18]. We present here a superposition of two dichroic rugate filters. Figure 6(a) shows the refractive index profiles consisting of two rugate filters centered around 1500 nm and 1900 nm with 63 and 50 periods, respectively. The combined index profile is apodized and index matched in the same way as the previous samples. The measured polarization-resolved transmittance of the two-line rugate filter is shown in Fig. 6(b). Two stop-bands appear and their positions depend strongly on the polarization direction of the incident light. In spite of the very complex index profile, the higher-order harmonics are well controlled and the sidelobes are rather small. The stop-band position, the width and the number can be tailored simply by properly controlling the rugate structures constructing the filter.

4. Conclusions

We have succeeded in producing Si-based dichroic rugate filters by the formation of sinusoidal refractive index profiles by electrochemical etching of (110) Si wafers. The filter had a stop-
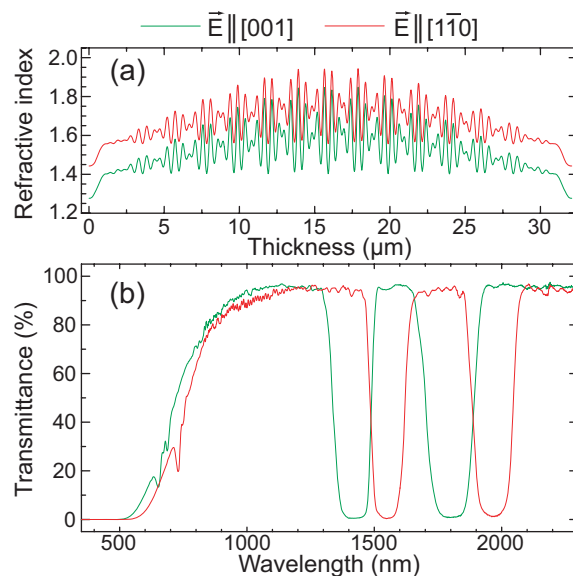

Fig. 6. Double band dichroic rugate filter centered around 1500 nm and 1900 nm with 63 and 50 periods, respectively: (a) refractive index profiles versus physical depth, (b) calculated and (c) measured polarization-resolved transmittance spectra for **E** parallel to the $[1\bar{1}0]$ and $[001]$ directions.

band depending on the polarization direction of the incident light without higher-order harmonics and sidelobes. The filters act as a high quality planar linear polarizer that can be used for high power lasers since there is no absorption of incident light in near infrared region. In the present procedure, the position and the width of stop-bands can easily be controlled. Furthermore, designs of complex structures can be achieved in a single step by combination of different dichroic rugate filters.

Acknowledgment